



SINGLE-MODE RAMAN FIBER LASER IN A MULTIMODE FIBER

THESIS

Matthew B. Crookston, 2Lt, USAF

AFIT/GAP/ENP/03-03

DEPARTMENT OF THE AIR FORCE
AIR UNIVERSITY

AIR FORCE INSTITUTE OF TECHNOLOGY

Wright-Patterson Air Force Base, Ohio

APPROVED FOR PUBLIC RELEASE; DISTRIBUTION UNLIMITED

The views expressed in this thesis are those of the author and do not reflect the official policy or position of the United States Air Force, Department of Defense, or the U.S. Government

Single-Mode Raman Fiber Laser in a Multimode Fiber

THESIS

Presented to the Faculty

Graduate School of Engineering and Management

Air Force Institute of Technology

Air University

Air Education and Training Command

In Partial Fulfillment of the Requirements for the

Degree of Master of Science (Applied Physics)

Matthew B. Crookston, BS

Second Lieutenant, USAF

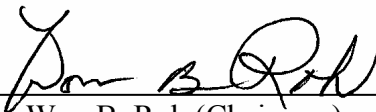
March 2003

APPROVED FOR PUBLIC RELEASE; DISTRIBUTION UNLIMITED

Single-Mode Raman Fiber Laser in a Multimode Fiber


Matthew B. Crookston, BS
Second Lieutenant, USAF

Approved:



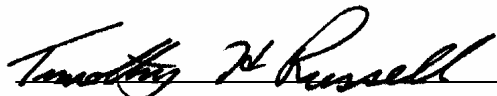
Won B. Roh (Chairman)

6 Mar 2003
Date



Glen P. Perram (Member)

10 Mar 2003
Date



Timothy H. Russell (Member)

6 MAR 2003
Date

Acknowledgments

I would like to thank the chair of my thesis committee, Dr. Roh, and the committee members Dr. Perram and Dr. Russell for their guidance and valuable input. I would also like to thank Dr. Baek and Shawn Willis for their help in the lab. Finally, I would like to thank my parents and especially my wife for all of their emotional support and encouragement.

Matthew B. Crookston

Table of Contents

Acknowledgments.....	iv
List of Figures.....	vii
List of Tables	ix
Abstract.....	x
Single-Mode Raman Fiber Laser in a Multimode Fiber.....	1
1 Introduction.....	1
2 Background.....	4
2.1. Stimulated Raman Scattering (SRS) in Optical Fibers.....	4
2.2. Raman Fiber Lasers (RFL)	6
2.3. Beam Quality	8
3 Experiment.....	10
3.1. Beam Quality Measurements.....	10
3.2. Energy and Spectrum Measurements.....	13
4 Beam Cleanup.....	14
4.1. Single Pass SRS Beam Cleanup	14
4.1.1. 300m Fiber Single Pass SRS Beam Cleanup.....	14
4.1.2. 40m Fiber Single Pass SRS Beam Cleanup.....	16
4.2. Free Running Laser Beam Cleanup	17
4.3. Beam Cleanup Summary	18
5 Energy and Spectral Analysis	20
5.1. Single Pass SRS Analysis.....	20

5.1.1.	300m fiber Single Pass SRS Analysis	20
5.1.2.	40m Fiber Single Pass SRS Analysis	24
5.2.	Raman Fiber Laser Analysis.....	27
6	Conclusion	31
	Appendix A: Numerical Approach for Estimating M^2	34
	Appendix B: Intensity Stabilization using a GaAs Wafer	37
	References.....	41
	Vita.....	43

List of Figures

Figure 1: The SRS process where a pump photon of frequency ν_p is annihilated and a down shifted Stokes photon ν_s , and optical phonon ν_o , are generated.	4
Figure 2: (a) Example of transmitted spectrum where each Stokes peak is separated by approximately 440 cm^{-1} . (b) Examples of far-field Stokes images dispersed by a diffraction grating. (c) Photograph of escaping light from fiber spool during data collection. Image from Ref 2.	5
Figure 3: The Fiber Bragg Grating showing reflection of the Bragg wavelength. Light and dark regions represent variations in index.	7
Figure 4: Example of a Raman fiber laser with fiber Bragg gratings.	8
Figure 5: A Schematic of the setup used to measure beam quality of separate Stokes beams.	10
Figure 6. Transmission Spectrum of fiber Bragg gratings obtained from BRAGG Photonics.	12
Figure 7. A Schematic of the setup used to make energy and spectrum measurements.	13
Figure 8. Example of spot size measurements and least squares fit to determine the M^2 values for the 300m fiber. M^2 Results: Pump = 20.88, 1 st Stokes = 9.41, 2 nd Stokes = 6.64, 3 rd Stokes = 6.55.	15
Figure 9: Near field pump beam profile showing a predominant LP_{11} mode.	17
Figure 10. Spectrum of 300m fiber with input energy near $350\mu\text{J}$	20
Figure 11. Evolution of the Stokes beams in the 300m fiber.	21
Figure 12. Fractional energies in the 300m fiber.	22
Figure 13. Output energy versus input energy for 300m fiber.	23
Figure 14. Evolution of the Stokes beams in the 40m fiber.	24
Figure 15. Spectrum of the 40m fiber output with a Q-switched pump.	25
Figure 16. Fractional output energies of the 40m fiber with a Q-switched pump.	26
Figure 17. Output vs Input energy for 40m fiber.	26

Figure 18. Spectrum of Raman Fiber Laser showing resonance at 1115nm.	28
Figure 19. Evolution of the 1 st Stokes in the RFL.	29
Figure 20. Fractional energy of the RFL.	29
Figure 21. Output energy versus input energy for the RFL.	30
Figure 22. Free running laser pulse comprised of a number of spikes and a width of about 50μsec.	37
Figure 23. Two-photon absorption in GaAs that has a bandgap of 1.42 eV.....	38
Figure 24. Setup testing the effectiveness of a GaAs wafer to reduce spikes in a free running laser pulse.	39

List of Tables

Table 1. Wavelengths for different Stokes from a 1064-nm pump wavelength, each separated by 440cm^{-1}	5
Table 2. Summary of M^2 measurements.....	19

Abstract

The feasibility of a transverse single-mode Raman fiber laser using a multimode fiber has been investigated. The Raman fiber laser operates in low-order transverse modes despite the fact the fiber supports multimode beam propagation. The performance characteristics of the Raman Fiber Laser are compared with those of the single-pass SRS beam.

Single-Mode Raman Fiber Laser in a Multimode Fiber

1 Introduction

As the Department of Defense transforms to meet the challenge of asymmetric warfare in combating terrorism, most reports recognize the importance of Directed Energy.¹ While there are many applications for lasers in this transformation vision, beam quality will limit the effectiveness of many of these applications. For example, a laser used to illuminate a target will have a longer range if it has a Gaussian profile. Any other profile will diverge faster than a Gaussian laser beam, and limit the range of the laser. Currently, solid-state lasers are one of the choices to produce high power lasers, but they also tend to be highly aberrated.^{1,2} Therefore, research into processes that clean up laser beams becomes important.

The idea to use nonlinear effects in multimode fiber as a tool for beam clean up began with the observation of picosecond Raman pulses with small spot sizes.³ Bladeck et al. used a mode-locked Nd:YAG laser to produce 25psec pulses at 532nm wavelength coupled into a 7.5m long multimode fiber with a 100 μ m core diameter. They observed that the diameter of the Stokes beams generated through Stimulated Raman Scattering (SRS) were about 10 times smaller than the pump beam. This smaller spot size suggested single-mode operation in a multimode fiber. Later, a mode locked and Q-switched Nd:YAG laser, operating with a wavelength of 1064 nm, produced a 150psec pulse with

a peak power of 600kW, and was focused into a 50m long multimode fiber that had a parabolic refractive-index profile and a core diameter of 50 μ m. In this experiment, Grudinin et al. observed the excitation of 12-15fsec SRS pulses in the multimode fiber.⁴ Motivated by these two experiments, Chiang studied the evolution of modes in the Stokes wave. Using a tunable dye laser operating at 585nm with 3nsec pulse widths focused into a 30m long, graded index multimode fiber with a 50 μ m core diameter, he observed that under the proper launching conditions, the Stokes wave propagated predominantly in the LP₀₁ mode. Chiang further predicted the possibility of a single-mode Raman fiber laser in a multimode fiber that could give higher power because of the larger spot size.⁵ In summary, all three of these references pointed out that one of the applications of these results could be the propagation of a single-mode Raman laser beam in a multimode fiber.

More recent research has verified beam cleanup through SRS and the related nonlinear process of Stimulated Brillouin Scattering.^{2,6,7} Using the second harmonic of a Nd:YAG laser operating at 532nm and a 300m long fiber, 10.5nsec pulses with about 160kW peak power, Russell et al. measured the beam quality of the combined Stokes beams. The authors reported an M^2 value of 20.7 for the transmitted pump beam and 2.4 for the combined Stokes beams.² The report further suggested that the beam quality improves for higher order Stokes because the far-field divergence pattern narrowed for higher order Stokes as seen in Figure 2(b) in Chapter 2. The first part of this research, described in Chapter 4, explores quantitatively the improvement of beam quality of the individual orders of the Stokes beam for single pass SRS. The second half of this

research described in Chapter 5, examines the Raman Fiber Laser in a multimode fiber.

Chapter 2 contains background information and Chapter 3 the experimental setup.

2 Background

2.1. Stimulated Raman Scattering (SRS) in Optical Fibers

Stimulated Raman Scattering (SRS) is a third order nonlinear, inelastic scattering process occurring in certain materials. The annihilation of an incident pump photon creates a lower frequency photon, referred to as the Stokes, and an optical phonon in that material.⁸ Figure 1 shows an energy conservation property of the SRS process.

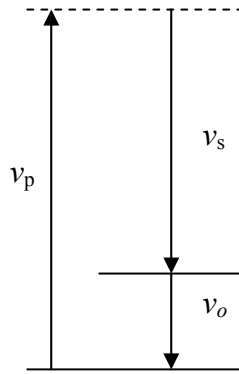


Figure 1: The SRS process where a pump photon of frequency ν_p is annihilated and a down shifted Stokes photon ν_s , and optical phonon ν_o , are generated.

The frequency shift of the Stokes photon is equal to the molecular vibrational frequency of the material. The Raman gain for silica fiber peaks around 440cm^{-1} . SRS in silica fibers was first observed using a frequency doubled Nd:YAG that produced 532nm emission. By coupling this light into a 9m fiber with a $4\mu\text{m}$ diameter, the output consisted of a 532nm beam and a 545nm Stokes beam.⁹ As seen in Figure 2, the Stokes beam itself can reach large enough intensity to act as a pump to produce a 2nd Stokes beam, and the 2nd Stokes beam can produce another Stokes beam so that with large

enough input energy, many order stokes beams each separated by 440cm^{-1} are produced. For a pump that has a wavelength of 1064nm , Table 1 lists the calculated values of the Stokes wavelengths assuming the peaks are separated by 440cm^{-1} .

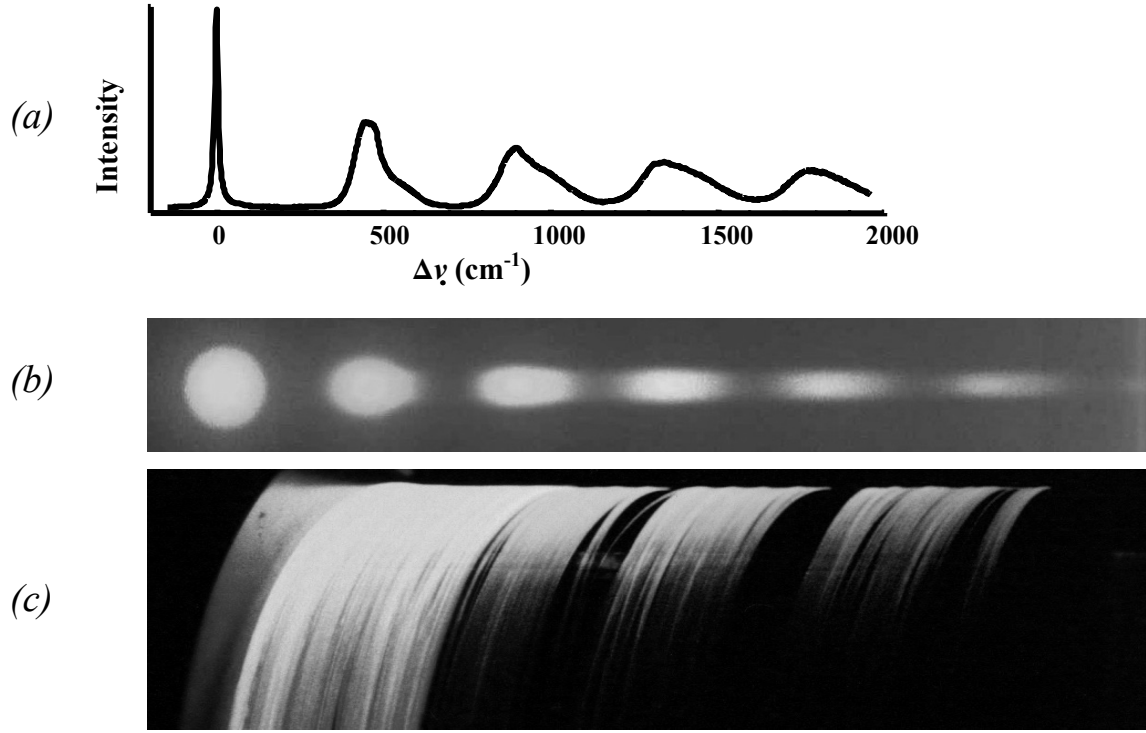


Figure 2: (a) Example of transmitted spectrum where each Stokes peak is separated by approximately 440cm^{-1} . (b) Examples of far-field Stokes images dispersed by a diffraction grating. (c) Photograph of escaping light from fiber spool during data collection. Image from Ref 2.

Table 1. Wavelengths for different Stokes from a 1064-nm pump wavelength, each separated by 440cm^{-1} .

Stokes	Wavelength [nm]
0-pump	1064
1st	1116
2nd	1174
3rd	1238
4th	1309
5th	1389
6th	1480

In optical fibers, the critical pump power, P_{cr} , required to reach SRS threshold is proportional to the effective area, A , and inversely proportional to the effective length of the fiber, L_{eff} .⁸

$$P_{cr} \propto \frac{A}{L_{eff}} \quad (2-1)$$

$$\text{where } L_{eff} = \frac{1}{\alpha_p} \left[1 - e^{-\alpha_p L} \right]$$

L is the fiber length and α_p is the fiber loss at the pump frequency. Therefore, fibers with longer lengths or smaller effective areas exhibit lower SRS thresholds. After the fiber is pumped with sufficient power to reach threshold for SRS, nearly all of the additional power goes into the generation of Stokes beams. For purposes of beam cleanup, the threshold represents the amount of power ‘lost’ in the conversion process.

Another important note, as mentioned by Chiang, is that the growth of a particular mode in a Stokes wave depends on the modal overlaps between the Stokes mode and the pump mode.⁵ Therefore, for best results in beam cleanup, the predominant mode of the pump should be the LP_{01} mode.

2.2. Raman Fiber Lasers (RFL)

To create a Raman fiber laser (RFL), mirrors that reflect the Stokes wavelength are placed at both ends of an optical fiber. Originally, a RFL was made by butting the fiber end directly to a mirror. The current method used is to use Fiber Bragg Gratings (FBG) written in the fiber to reflect the Stokes wavelength.¹⁰ Of the four different processes currently used to fabricate FBGs, all of them irradiate the fiber with a sinusoidal intensity pattern of UV radiation. Due to the photosensitive nature of the fiber, the regions

exposed to higher intensity undergo larger changes to the optical index.¹¹ Figure 3 shows the periodic nature of the index as it is written in the fiber, where Λ is one period of the index change. The Bragg wavelength, λ_B , that will have the highest reflection due to the grating, is related to Λ by*:

$$\lambda_B = 2\Lambda. \quad (2-2)$$

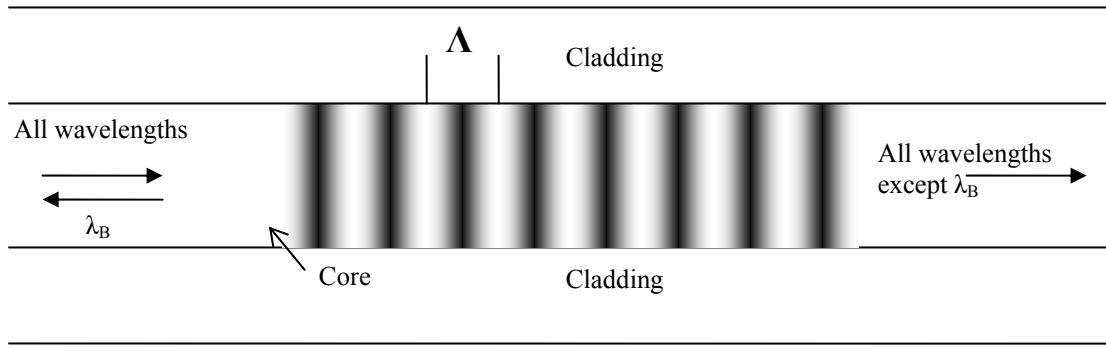


Figure 3: The Fiber Bragg Grating showing reflection of the Bragg wavelength. Light and dark regions represent variations in index.

Writing these gratings in the fiber at both ends to reflect the Stokes beam creates a Raman fiber laser. Figure 4 shows a schematic diagram of a Raman fiber laser. Light coupled from a pump laser into a fiber generates SRS. If the pump beam has a long enough duration, the Stokes wave will oscillate between the two FBG and produce a RFL.

* This is derived from the Bragg angle equation: $\sin \theta_B = \frac{\lambda}{2\Lambda}$, where $\theta_B = 90$ degrees.

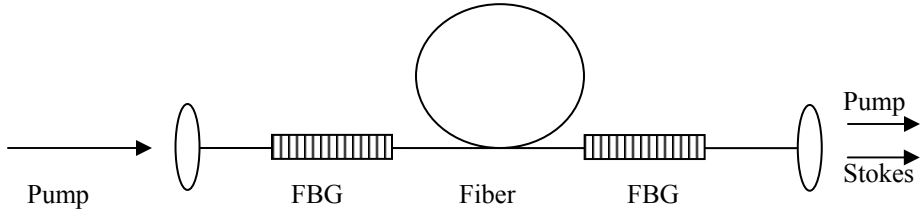


Figure 4: Example of a Raman fiber laser with fiber Bragg gratings.

2.3. Beam Quality

Since a Gaussian beam has the best laser beam propagation characteristics, laser beam quality values compare the laser beam to a Gaussian laser beam. A Gaussian laser beam propagates according to the following equation:

$$w^2(z) = w_0^2 + \frac{\lambda^2}{\pi^2 w_0^2} (z - z_0)^2, \quad (2-3)$$

where $w(z)$ is the spot size of the beam, w_0 is the beam waist, z_0 is the beam waist location, and λ is the wavelength of the laser. Siegman¹² proposed that a factor, M^2 , could be added to the above equation to describe the propagation of a real laser beam, such that:

$$w^2(z) = w_0^2 + (M^2)^2 \frac{\lambda^2}{\pi^2 w_0^2} (z - z_0)^2, \quad (2-4)$$

where M^2 is the value that compares the laser beam to that of a Gaussian laser beam, and the value $M^2 = 1$ corresponds to a Gaussian laser beam. The practical way this is measured is to take at least three spot size measurements of the beam at different

locations and fit the values of M^2 , z_0 , and w_0 . Appendix A outlines a least squares method for calculating these values from measured spot sizes. To measure the spot size, this research utilized a frame grabber system with the software program *BeamView* produced by the Coherent Auburn Division.¹³ *BeamView* performs a least squares fit of an acquired laser beam profile to the equation

$$I = V \left[\exp \left(- \frac{(x-c)^2}{\sigma} \right) \right]^2, \quad (2-5)$$

where I is the intensity of a pixel at location x , V is the maximum intensity of the fitted Gaussian curve, c is the center of the Gaussian fit peak, and σ is the radius of the Gaussian Fit curve at $1/e^2$ intensity level. This last term, σ , is taken as the value for the spot size of the laser beam.

A quick way to estimate the M^2 value that a fiber will support is to compare the acceptance angle of the fiber to the divergence angle of a Gaussian beam that has a waist equal to the diameter of the fiber core. The acceptance angle of the fiber, θ_f , is given by $\theta_f = \sin^{-1}(NA)$, where NA is the numerical aperture of the fiber. The divergence angle of a Gaussian beam with waist d is given by $\theta_g = 2\lambda / \pi d$, where λ is the wavelength of the beam. As an example, the M^2 of a fiber that has a 50 μm core diameter, NA = 0.20, and is guiding 1064nm light would be estimated by:

$$M^2 \approx \frac{\theta_f}{\theta_g} \approx \frac{\pi d \sin^{-1}(NA)}{2\lambda} \approx 15.$$

3 Experiment

3.1. Beam Quality Measurements

To explore the differences between single-pass SRS to SRS in a Raman fiber laser, this research used two experimental configurations. The first set-up, depicted in Figure 5, is used for measuring beam quality. The fiber is pumped by a 10Hz Continuum Surelite Nd:YAG laser operating at 1064nm. This laser operates Q-switched for the single-pass experiments, and free running for the RFL experiment. The pulse width for the Q-switched operation is $7\text{nanoseconds} \pm 0.6\text{ns}$, and free running, it produces a series of spikes over a pulse width of $51\mu\text{sec} \pm 5\mu\text{sec}$.[†]

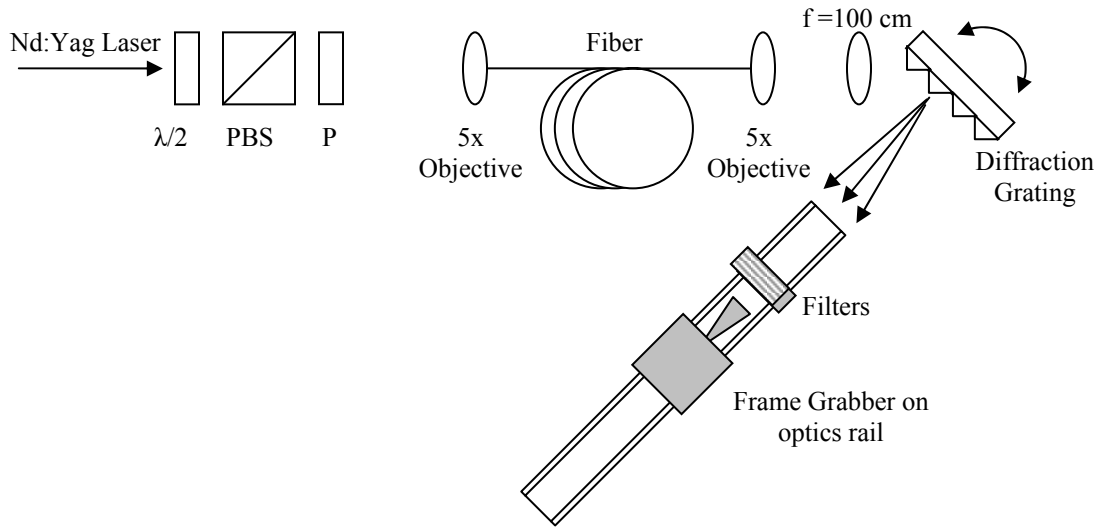


Figure 5: A Schematic of the setup used to measure beam quality of separate Stokes beams.

[†] Pulse width error calculated from standard deviation of the pulse width.

Since the power from the laser may easily damage the fiber and since it is necessary to vary the input intensity into the fiber to analyze the growth of the Stokes beam, three optical elements regulate the input energy to the fiber: a half-wave plate, Polarizing Beam Splitter (PBS), and polarizer. The laser emits horizontally polarized light. The PBS passes horizontally polarized light. A half-wave plate on a rotating stage is placed between the laser and the PBS to attenuate the output energy of the laser. The half-wave plate is set to limit the maximum power just below the fiber damage threshold. (If the half-wave plate is rotated more than three degrees, the transmitted energy damages the front end of the fiber. Rotating the half-wave plate only 2 degrees reduces the likelihood the energy from the laser will damage the fiber.) Inserting a polarizer after the PBS allows the rotation of the polarizer to adjust the energy of the pump transmitted to the fiber.

From the half-wave plate, PBS, and polarizer combination, the light from the laser is coupled into the fiber by a 5x microscope objective. This microscope objective has a Numerical Aperture (NA) = 0.13. The graded index fiber, manufactured by Corning, has a core diameter of $50\mu\text{m} \pm 3\mu\text{m}$ with a 0.200 ± 0.015 NA. At 1064 nm, the fiber has an effective index of 1.488 ± 0.001 and an attenuation coefficient, $\alpha = 1.08\text{dB}/\text{km} = 0.25\text{km}^{-1}$. Two lengths of fiber were used, a 300m fiber and a 40m fiber. The 40m fiber has fiber Bragg gratings (FBG) written on both ends. Figure 6 is the transmission spectrum of the combined FBGs as received from BRAGG Photonics that made the FBGs. The peak reflection is at 1115.1nm.

BRAGG Photonics

TCWL: 1115.11 nm
Reflectivity: 99.61 %
FWHM: 2.01 nm

Inspected by:

Reference number: 4099

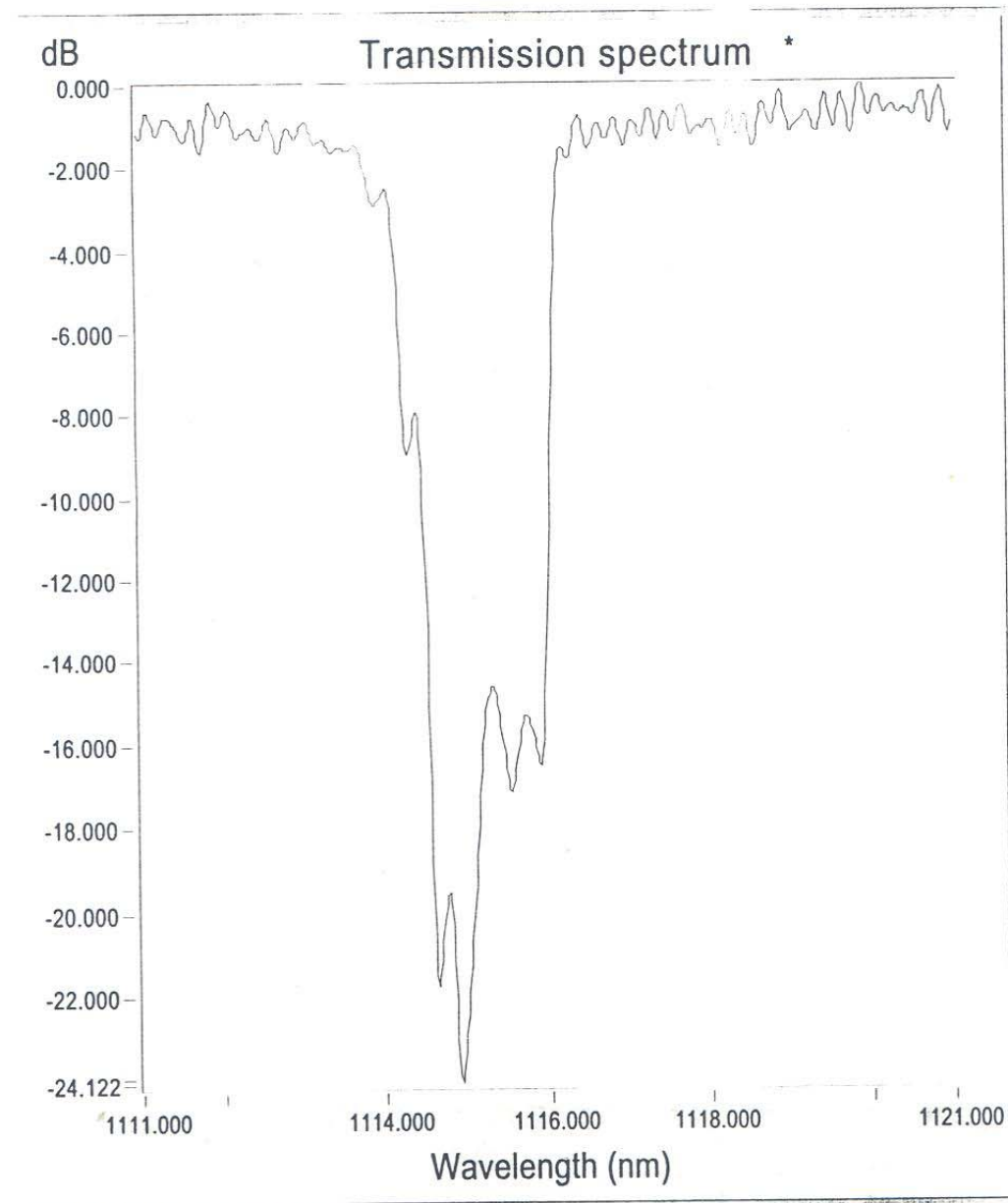


Figure 6. Transmission Spectrum of fiber Bragg gratings obtained from BRAGG Photonics.

At the output end of the fiber, a 5x microscope objective collimates the light. A 100cm positive lens focuses the beam to an optics rail. A diffraction grating with 295 grooves/mm and a blaze angle of $1.34\mu\text{m}$ separates the pump and Stokes beams. A frame grabber system with an Electrophysics 7290 PbS camera on an optics rail measures the beam waist at different locations.

3.2. *Energy and Spectrum Measurements*

The second set-up is depicted below in Figure 7. This set-up is very similar to the set-up used to take beam quality measurements, except the positive lens, diffraction grating, and a camera on an optics rail are replaced with an energy meter and spectrum analyzer.

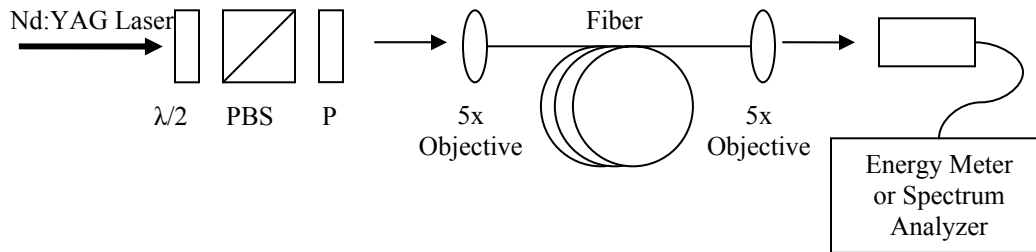


Figure 7. A Schematic of the setup used to make energy and spectrum measurements.

Energy measurements are taken with a *Laser Probe* energy meter and spectral measurements are taken with an ANDO Optical Spectrum Analyzer. The spectrum analyzer has a range from 350 – 1750nm and configured for 1nm resolution in these experiments.

4 Beam Cleanup

One of the main objectives of this research is to analyze the improvement of beam quality in the higher order Stokes beams. As depicted previously in Figure 5, a diffraction grating separates the pump beam from the Stokes beams. Individually, the beams are focused along an optics rail. A frame grabber measures the spot size of the beam at different locations along the rail. Because the diffraction grating spreads the beam in the horizontal direction, or ' x ' axis, the diameter of the beam is measured along the vertical ' y ' axis. At each position, the diameter of the beam was measured from the average of at least 50 acquired images. Section 2.3 outlines the process used to calculate the M^2 values from the diameter of the beam at several locations. The first section in this chapter reports the measurements of beam cleanup for single pass SRS in both the 300m and 40m fibers. For these measurements, the laser is Q-switched. In the second section of this chapter, the pump laser is altered to free running operation so that the much longer pulse width allows the first Stokes energy in the 40m fiber to be amplified between the fiber Bragg gratings (FBG) like a laser oscillator.

4.1. *Single Pass SRS Beam Cleanup*

4.1.1. 300m Fiber Single Pass SRS Beam Cleanup

Figure 8 shows an example of spot size measurements along with a least squares fit for the 300m fiber.[‡] The figure shows that the beam waist for the Stokes is about half the

[‡] See Appendix for more information on the numerical method used to fit the data.

pump waist. In addition, waist locations for the higher order stokes are shifted to the left compared to the waist location of the pump. The calculated M^2 values from the test shown in the figure are: Pump = 20.88, 1st Stokes = 9.41, 2nd Stokes = 6.64, 3rd Stokes = 6.55, and 4th Stokes = 6.14 [not shown].

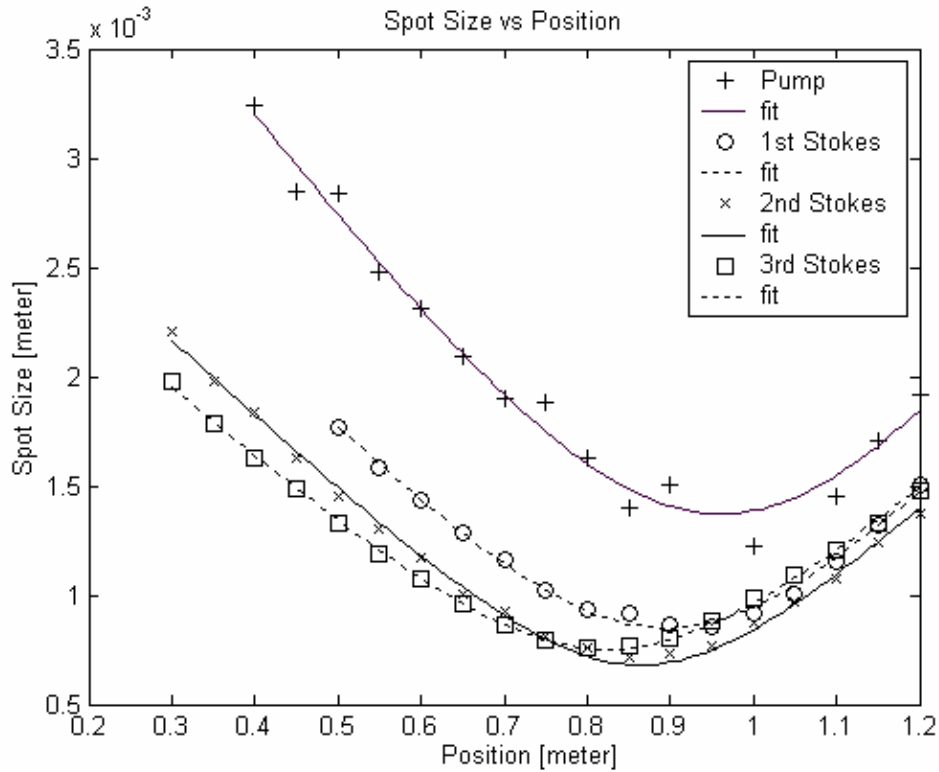


Figure 8. Example of spot size measurements and least squares fit to determine the M^2 values for the 300m fiber. M^2 Results: Pump = 20.88, 1st Stokes = 9.41, 2nd Stokes = 6.64, 3rd Stokes = 6.55.

The unexpectedly high M^2 value for the first Stokes of 9.41 prompted a second test. The 300m fiber was cleaved, stripped, and realigned. The results for the second test gave the following M^2 values for the different beams: Pump = 13.38, 1st Stokes = 5.51, 2nd Stokes = 3.82, and 3rd Stokes = 4.00.

In these two tests, the first Stokes beam is about a factor of two better than the pump beam and the second Stokes is about a factor of $\sqrt{2}$ better than the first Stokes beam. The beam quality values for higher order Stokes could not be taken because the peaks of the higher order Stokes could not be resolved from the background on the camera.

4.1.2. 40m Fiber Single Pass SRS Beam Cleanup

One major difference between the 300m fiber and the 40m fiber is that the longer fiber produced more orders of Stokes than the shorter fiber. For the shorter fiber, it was difficult to measure the spot size for more than the first two Stokes beams because the 3rd Stokes beam was either below or barely above threshold. The first measurement of beam quality yielded the poor result of the pump $M^2 = 9.14$ and the 1st Stokes $M^2 = 6.45$. This poor beam quality for the first Stokes beam is caused by the pump beam propagating in a predominantly LP_{11} mode as seen in Figure 9. Since the Stokes beam grows in the predominant mode of the pump, the pump should have a predominant LP_{01} mode for the most effective beam cleanup.⁵ This makes proper alignment of the fiber crucial. To align the fiber, an energy meter was placed at the output and the fiber was aligned for maximum output energy. A more effective way to align the fiber is to use the frame grabber and maximize the peak of the Stokes beam. Using this alignment procedure, another test of the beam quality resulted in M^2 values of, pump = 15.95, 1st Stokes = 2.14, and 2nd Stokes = 2.57.



Figure 9: Near field pump beam profile showing a predominant LP₁₁ mode.

4.2. Free Running Laser Beam Cleanup

In this experiment, the pump laser is operating free running so that it produces a pulse width of about 50 μ s. The beam quality of the output beams when pumped with a free running laser is very similar to the beam quality of the single pass SRS beam cleanup mentioned previously. The fitted M^2 values for the free-running configuration are: pump = 9.2, 1st Stokes = 2.6, and 2nd Stokes = 1.9. The improvement from the pump to the first Stokes is similar to the beam clean up of the 40m single pass experiment. The

improvement from the 1st Stokes to the 2nd Stokes shows an improvement of beam quality by a factor of about $\sqrt{2}$, similar to the results for the 300 m fiber.

4.3. Beam Cleanup Summary

For the single pass experiments, the two measurements with the 300 m fiber had M^2 values of the first Stokes approximately a factor of two better than the pump, and the second Stokes about a factor of $\sqrt{2}$ better than the first Stokes. In the first of three experiments with the 40m fiber, the pump propagated predominantly in LP_{11} mode and the first Stokes had only slightly better beam quality. In the other two experiments, the first Stokes had an M^2 value near 2. In the RFL, the first Stokes had an M^2 near 2, but also showed an improvement factor of about $\sqrt{2}$ in the second Stokes from the first Stokes. Table 2 lists the M^2 values obtained in each experiment.

It may be noted that a few of the M^2 values exceed the estimated high M^2 of around 15 as calculated in section 2.3. The M^2 values listed below are most likely inflated because the spot size of the beam was measured from the average of 50 images. Jitter in the laser causes the center of the beam to vary slightly from pulse to pulse. As the center of the beam varies slightly from pulse to pulse, the spot size of the average would be larger than the spot size of each individual shot. Further, this would have more of an effect in the far field where the spot size is larger. Since the M^2 value compares the far field divergence to the divergence of a Gaussian beam, over estimating the far field spot size would result in larger M^2 numbers.

Table 2. Summary of M^2 measurements.

fiber length	Pump Operation	Beam Quality [M^2]				notes
		pump	1st Stokes	2nd Stokes	3rd Stokes	
300m	Q-switched	20.88	9.41	6.64	6.55	
300m	Q-switched	13.38	5.51	3.82	4.00	
40m	Q-switched	9.14	6.50			Pump predominantly LP 1,1 mode
40m	Q-switched	7.99	2.33	3.74		
40m	Q-switched	15.95	2.14	2.57		
40m	Free running	9.20	2.60	1.90		

5 Energy and Spectral Analysis

5.1. Single Pass SRS Analysis

To analyze how the Stokes beams evolve, spectrum and energy measurements were taken as a function of input energy for both the 300m and 40m fibers with the laser Q-switched according to Figure 7.

5.1.1. 300m fiber Single Pass SRS Analysis

The pump and the first three Stokes beams are quickly identified on a spectrum from the output of the fiber. The peaks correspond closely to the values in Table 1 on page 5.

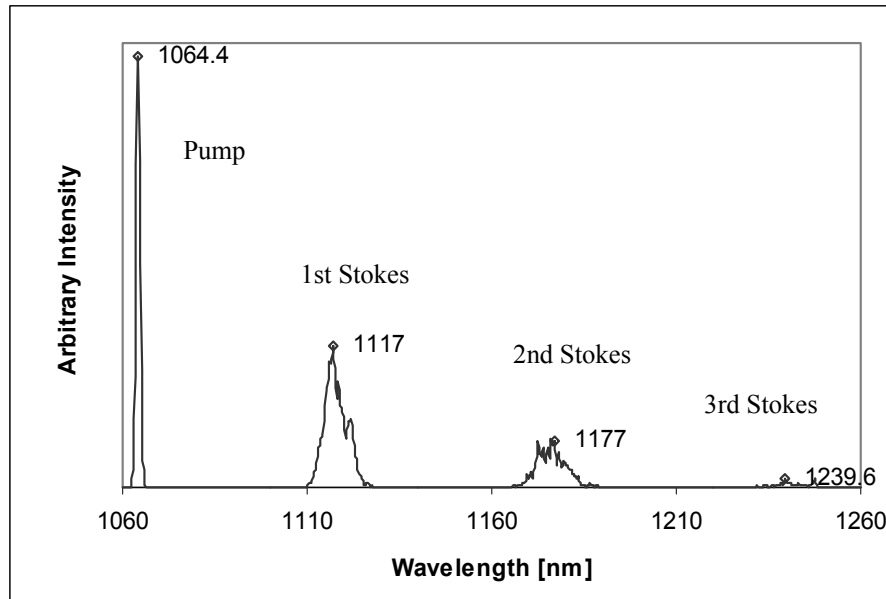


Figure 10. Spectrum of 300m fiber with input energy near 350 μ J.

To see the evolution of the Stokes in the 300m fiber, spectral measurements were taken at different input energies. Figure 11 shows the evolution of the Stokes beams in the 300m fiber. It can be seen on this graph that an increase in energy after the 1st Stokes reaches threshold that most of the energy goes into the growth of that beam.

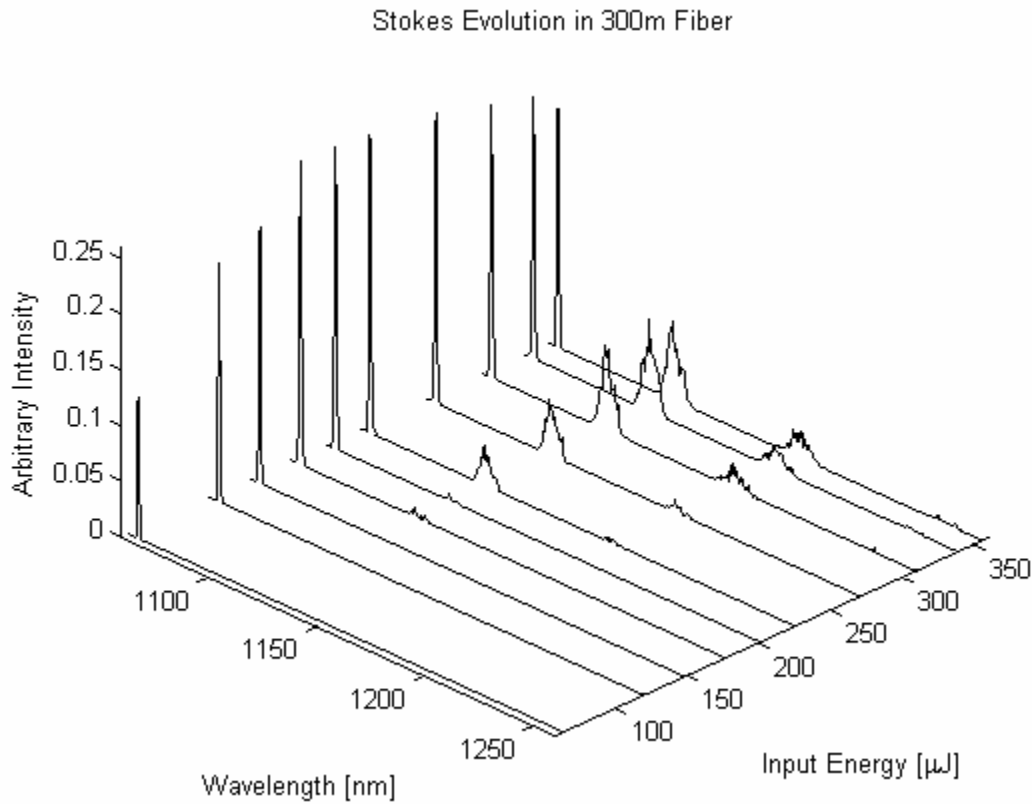


Figure 11. Evolution of the Stokes beams in the 300m fiber.

By calculating the area under each of the curves and dividing by the total area, fractional intensity may be calculated. Figure 12 shows the fractional energies as a function of input energy for the 300m fiber.

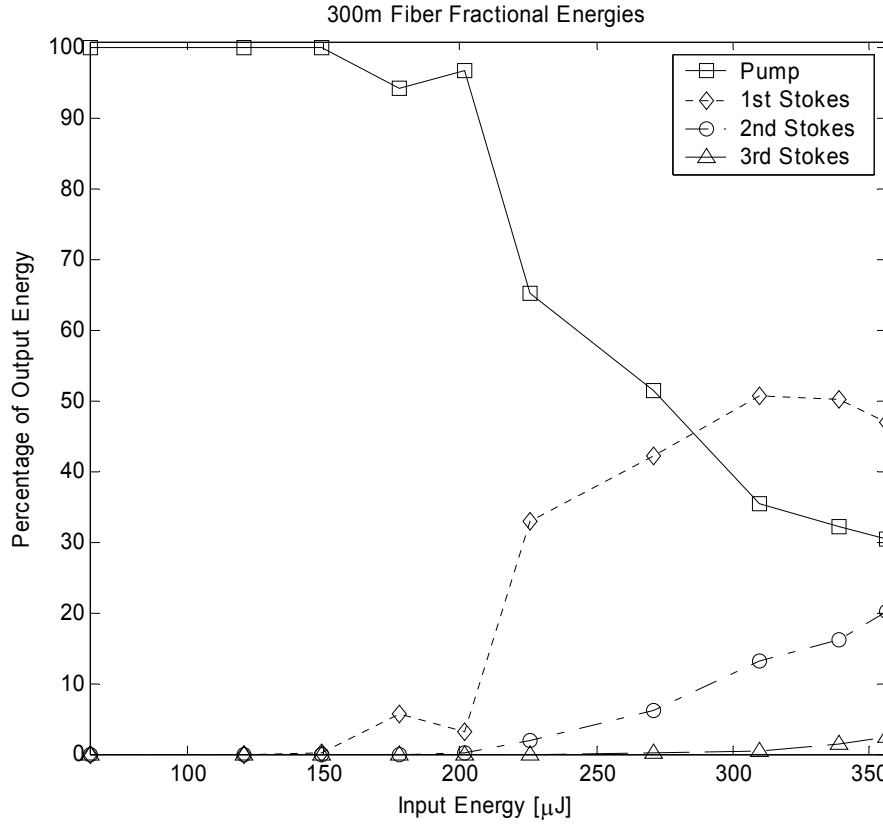


Figure 12. Fractional energies in the 300m fiber.

An energy meter placed before the spectrum analyzer measured the output energy from the fiber. By multiplying the fractional energy by the output energy, it is possible to create a graph of output energy versus input energy. Calculating the efficiency of the 1st Stokes conversion by dividing the output energy by the input energy gives an efficiency near 1.6 %. This is a very low efficiency and most likely due to misalignment. In order to estimate how well the pump beam is coupled into the fiber, the energy coupled into the fiber may be calculated using,

$$E_{out} = E_{in} \exp(-\alpha L), \quad (5-1)$$

where E_{out} is the measured output power from the fiber, E_{in} is the coupled energy into the fiber, α is the attenuation coefficient of the fiber, and L is the length of the fiber. The fiber has an attenuation coefficient, $\alpha = 2.5 \times 10^{-4} \text{ m}^{-1}$ and length = 300m. Examining the first data point in Figure 13, $E_{\text{out}} = 1.81 \mu\text{J}$ and therefore from equation 5-1, the actual energy coupled in to the fiber, $E_{\text{in}} = 1.95 \mu\text{J}$. Dividing E_{in} by the measured energy before the fiber of $64.6 \mu\text{J}$ indicates that only about 3% of the energy is being coupled into the fiber. Assuming that only 3% of the energy is being coupled into the fiber, the Stokes beam has a maximum conversion efficiency of around 54%.

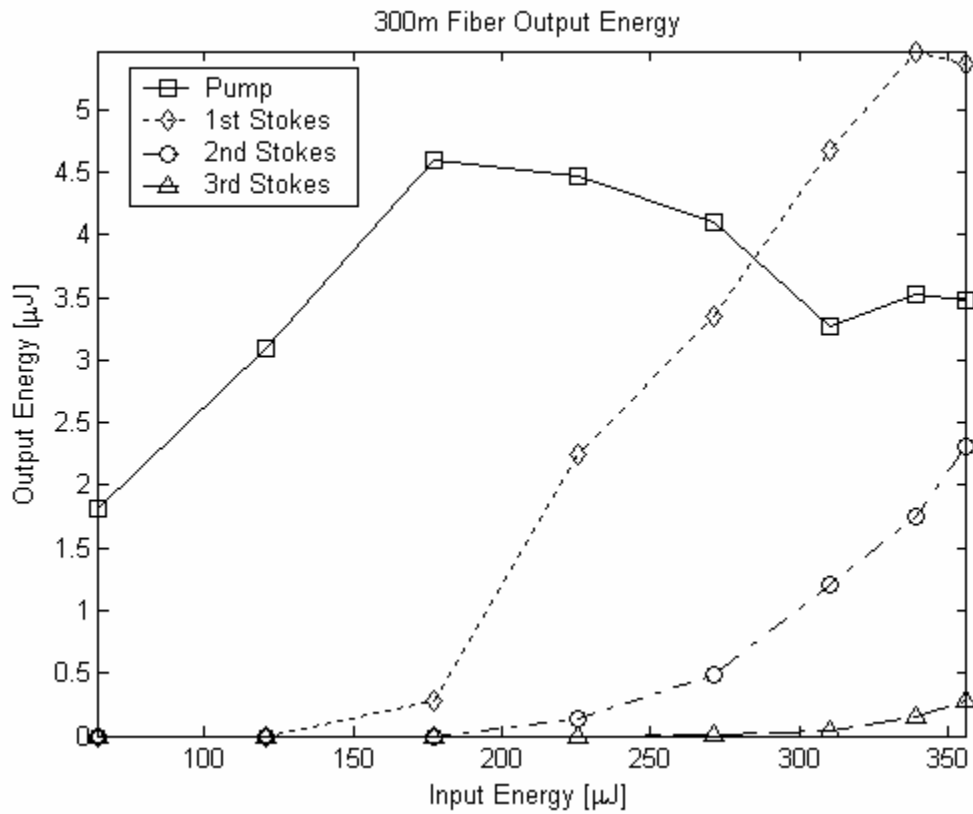


Figure 13. Output energy versus input energy for 300m fiber.

5.1.2. 40m Fiber Single Pass SRS Analysis

The 40m fiber has many similarities to the 300m fiber. One similarity is that the first Stokes beam reaches threshold for nearly the same input energy. According to equation 2-1, the Stokes beam in the shorter fiber should have a higher threshold, but as mentioned previously, the 300m fiber was not aligned well. The following graph shows the growth of the Stokes in the 40m Fiber.

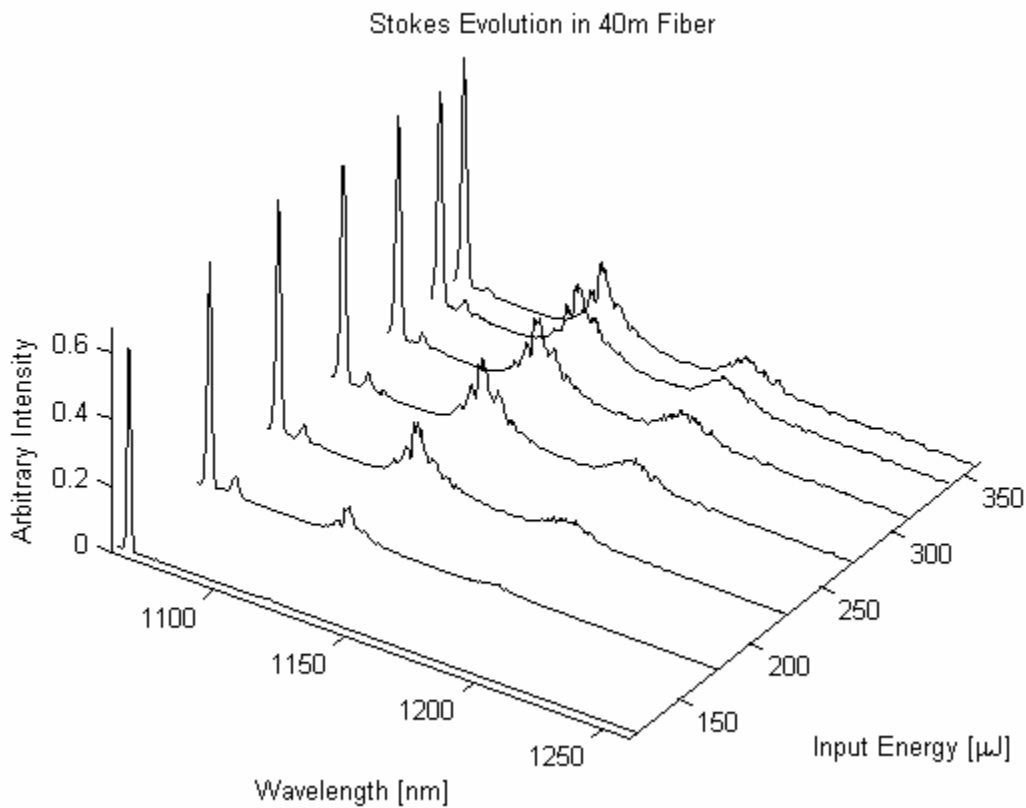


Figure 14. Evolution of the Stokes beams in the 40m fiber.

The following spectrum, taken at about 270 μ J input pump energy is different in many ways from the 300m fiber. First, the peak of the 1st Stokes is shifted to a higher wavelength. This is due to the reflection off the FBG, and confirmed by a local minimum

at 1115.4nm, the Bragg wavelength of the FBG. Second, the Stokes beam is spectrally wider in the 40m fiber than in the 300m fiber. Third, for the pump powers examined, only the first two Stokes reach threshold. Finally, a peak just to the right of the pump beam appears. This anomaly has a peak wavelength at 1074nm. By integrating the area under each of the peaks and dividing by the total energy, fractional energies are calculated and graphed in Figure 16. Multiplying the fractional energies by the output energy gives the output energy of each of the beams and is graphed in Figure 17. With the better alignment, the conversion efficiency into the first Stokes is near 10%. Once again, using equation 5-1 with $L = 40\text{m}$, and the first data point in Figure 17 (92.6, 16.38), it is determined that about 18% of the light is being coupled into the fiber. This also corresponds to a conversion efficiency of the energy coupled into the fiber to the first Stokes at about 55%.

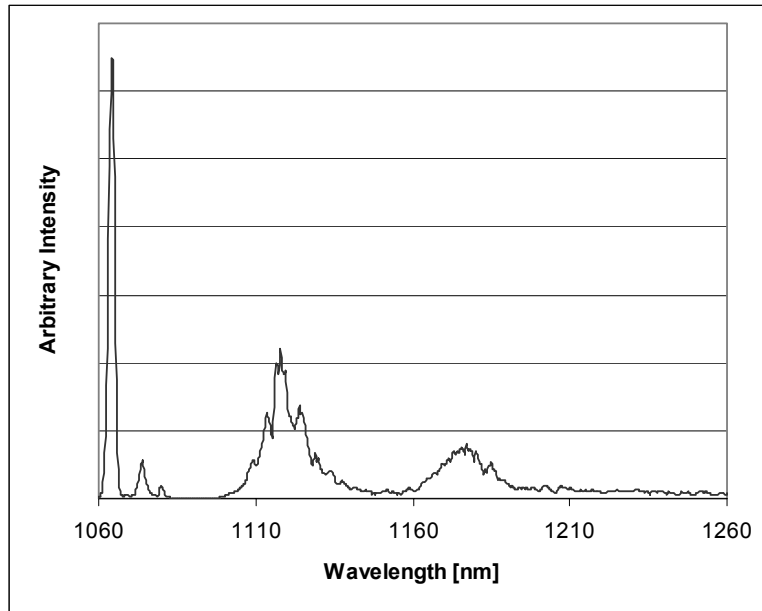


Figure 15. Spectrum of the 40m fiber output with a Q-switched pump.

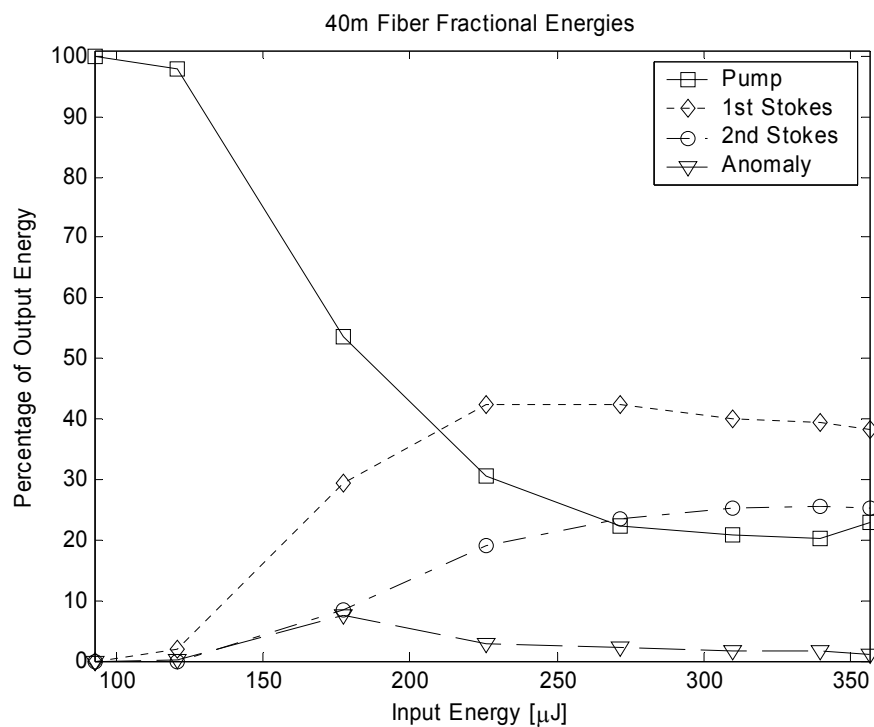


Figure 16. Fractional output energies of the 40m fiber with a Q-switched pump.

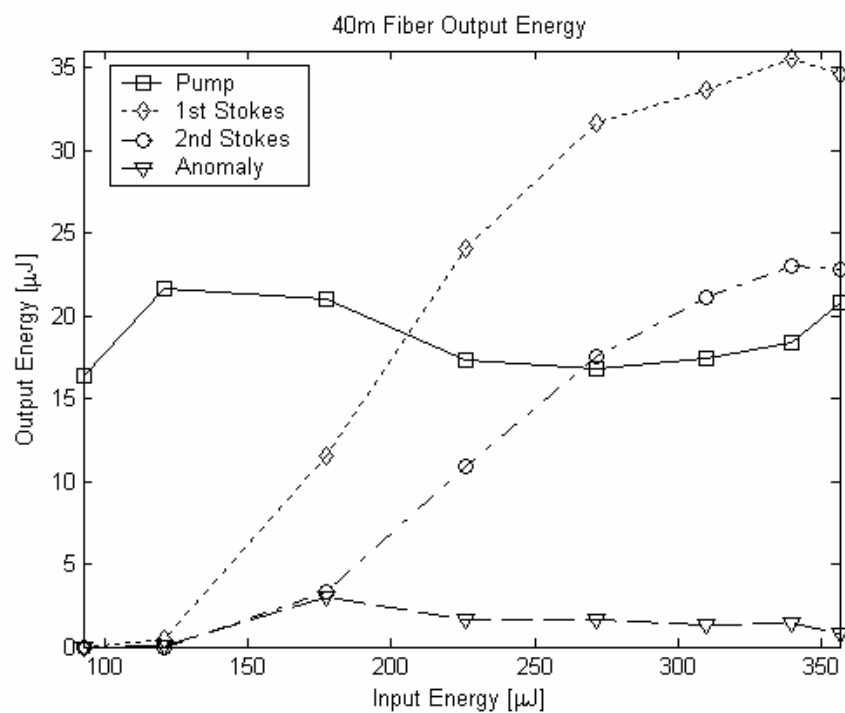


Figure 17. Output vs Input energy for 40m fiber.

5.2. Raman Fiber Laser Analysis

In order for feedback to occur in a Raman fiber laser, the pump pulse duration must be sufficiently long so that light in the fiber can make several round trips. As mentioned in Chapter 0, the free running laser has a pulse width of close to 50 μ s and the fiber has an effective group index of $n = 1.488$. The number of round trips may be approximated by,

$$N \approx \frac{ct}{n} \cdot \frac{1}{2L} \approx 125,$$

where N is the number of round trips, c is the speed of light, t is the pulse width, n is the index of the fiber, and $2L$ is the round trip length. This produces feedback for the laser. The feedback is confirmed by a spectrum of the 40m fiber. The peak of the first Stokes this time is centered on 1115nm, the Bragg wavelength. In addition, a full width half-max of about 2nm for the Stokes is much narrower than the 6nm FWHM for free running case and corresponds nicely to the FWHM of the reflectance of the Bragg Grating in the fiber.

The evolution of the Stokes beam in the RFL is shown in Figure 19. Since the Stokes intensity is much lower when compared to the pump and since the second Stokes has just reach threshold, this suggests that the Stokes beam is starting to evolve. Using the same process of integrating the areas under the curve, Figure 20 graphs the fractional values as a function of input power, and Figure 21 graphs output energy versus input energy.

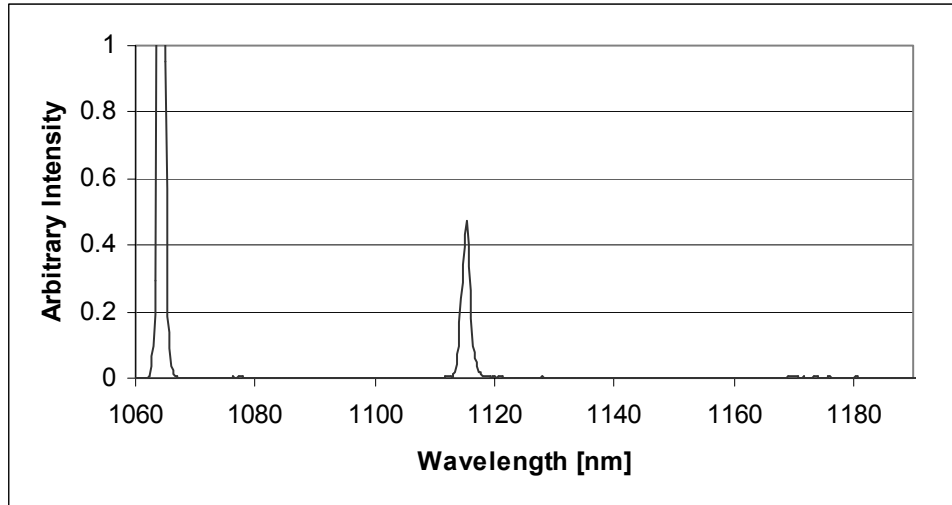


Figure 18. Spectrum of Raman Fiber Laser showing resonance at 1115nm.

Using equation 5-1 again, about 28% of the pump energy was coupled into the fiber. Of the light coupled into the fiber, 11% is converted to the first Stokes wavelength. This conversion is measured near the threshold of the second Stokes beam. In the previous two examples, the conversion of energy to the Stokes beam did not reach a maximum until there was much more energy than that required for the second Stokes to hit the threshold. Therefore, it is predicted that as more energy is coupled into the RFL the conversion of energy to the first Stokes would at least reach the conversion efficiency of the fiber when the pump is Q-switched.

One large difference between the RFL and the single pass experiments is that the threshold for the Stokes beam is much lower. The power to reach threshold for the RFL is about three orders of magnitude smaller than it is for the single pass SRS. The large reduction to threshold is attributed to the fact that the Bragg gratings provide feedback at the Stokes wavelength in the fiber.

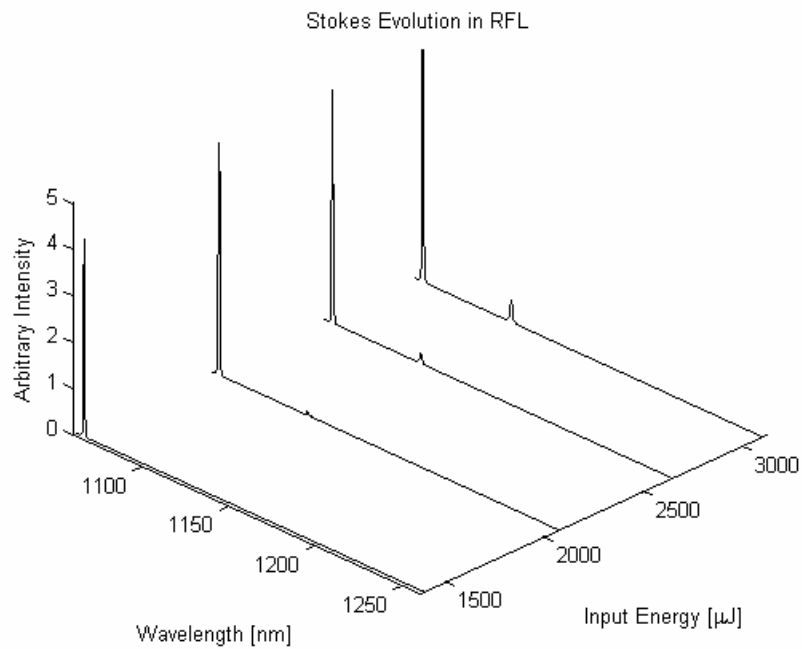


Figure 19. Evolution of the 1st Stokes in the RFL.

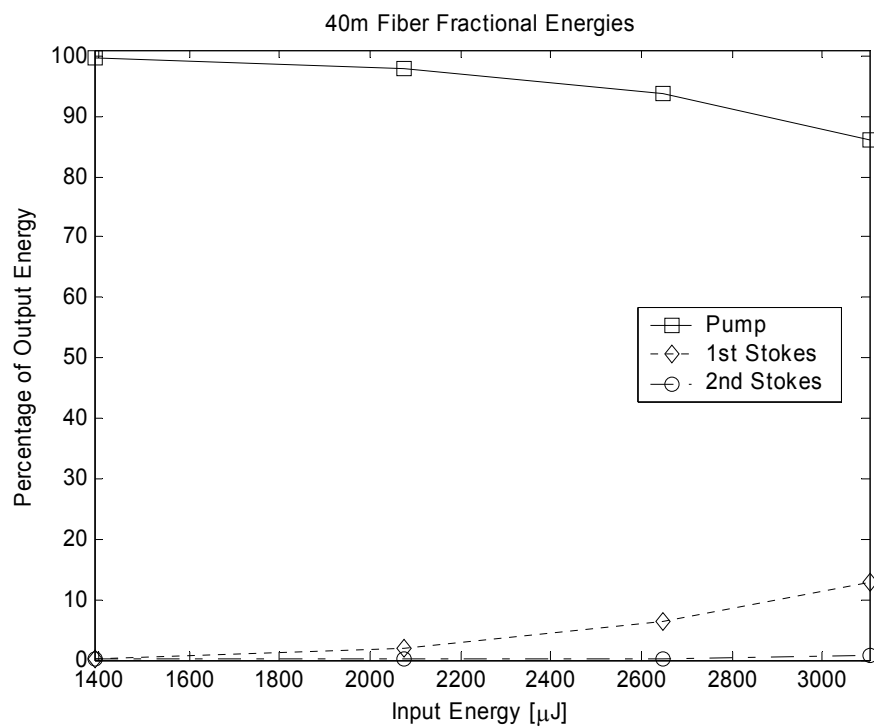


Figure 20. Fractional energy of the RFL.

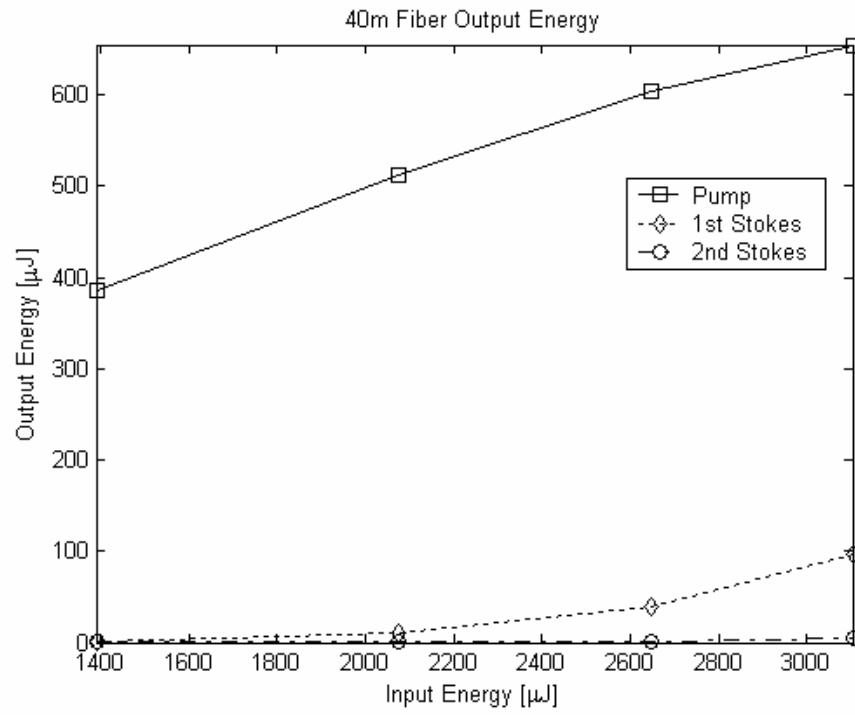


Figure 21. Output energy versus input energy for the RFL.

6 Conclusion

This research demonstrated a Raman fiber laser in a multimode fiber. To create the RFL, Bragg gratings were written in the optical fiber and act as mirrors to create an optical resonator. The fiber was end pumped by a free running Nd:YAG laser operating a 1064nm. The pulse width of the free running laser is 50 μ sec. Q-switched, the laser has a pulse width of about 7nsec. The RFL needed the longer pulse width so that the Stokes beam could be amplified as the light oscillated in the fiber between the Bragg gratings. When the pump laser was Q-switched, single pass SRS measurements were taken because the light did not oscillate in the fiber. Using the pump laser free running or Q-switched this research examined beam quality and spectrum analyzed of SRS in the fiber.

In the single pass experiments, the beam quality for the 300m fiber's first Stokes beam was about a factor of two better than the pump beam. The second Stokes was about a factor of $\sqrt{2}$ better than the first Stokes. For higher order Stokes, the beam quality showed marginal, if any, improvement. For the 40m fiber, three beam quality measurements were taken. In the first measurement, the pump was propagating predominantly in the LP₁₁ mode. The pump M^2 equaled 9.1 while the Stokes equaled 6.5. The poor cleanup is due to the energy not propagating in a predominantly LP₀₁ mode. In the other two experiments, care was given to better align the fiber. In those experiments, each of the pump beams had similar M^2 values to the pump beams in the 300m fiber, yet had Stokes beams M^2 values near 2. For the RFL, the M^2 value of the Stokes was near 2.5, but the Second Stokes in the RFL showed the best M^2 value of 1.9. In all of these experiments, the fiber had to be aligned as to make the pump beam propagate in

predominantly the LP_{01} mode. Furthermore, these values are expected to over estimate the true beam quality of the different beams because the spot sizes for the beams were measured from the average of many pulses of the laser. Since jitter in the laser caused the center of the beam to shift slightly at each measurement, the spot size of the average of the pulses was larger and resulted in larger M2 values.

In reviewing the spectra, the spectra of the 300m fiber did not show anything unusual. The peaks of the Stokes were very close to theoretical values. In the single pass experiment with the 40m fiber, the spectral widths of the peaks were wider than that of the corresponding peaks of the 300m fiber. In addition, a minimum in the first Stokes at the Bragg wavelength shifted the peak of the Stokes to a lower frequency. A peak at 1074nm showed up due to an unknown source. The Stokes beam of the RFL had a 2nm FWHM compared to the 6nm FWHM of the single pass 40m fiber. The Stokes beam was centered on the Bragg wavelength. This is in contrast to the dip at the Bragg wavelength for the single pass experiment and confirms oscillation in the fiber.

The conversion efficiency to the Stokes wavelength is important in any application that would use this process for laser beam cleanup. For the single pass SRS experiments, the conversion was near 55% of the light coupled into the fiber. For the RFL experiment, the conversion was near 11%. The RFL has lower conversion efficiency because it was not operating much above threshold. As the input energy is increased, it is expected that the conversion efficiency will be near, if not greater than that for the single pass SRS experiments.

It was also shown that the RFL reduced the threshold for SRS by about three orders of magnitude compared to a fiber of similar length. This reduction in threshold is from

the feedback of the Bragg gratings at the Stokes wavelength. This is an advantage because it reduces the threshold required to operate the Raman fiber laser.

The purpose of this research was to demonstrate a single-mode Raman fiber laser in a multimode fiber. The experiment came short in demonstrating that the Raman fiber laser was single-mode, but did demonstrate that the beam propagated in low-order transverse modes despite the fact it was in a multimode fiber.

Appendix A: Numerical Approach for Estimating M^2

Following the discussion in section 2.3, this appendix outlines a numerical approach for calculating the M^2 value of laser beam. According to reference 12, a real laser beam spot size is given by,

$$w^2(z) = w_0^2 + (M^2)^2 \frac{\lambda^2}{\pi^2 w_0^2} (z - z_0)^2, \quad (\text{A-1})$$

where $w(z)$ is the spot size of the beam, w_0 is the beam waist, z_0 is the beam waist location, z is the distance from the waist, λ is the wavelength of the laser, and M^2 is the value that compares the laser beam to that of a Gaussian laser beam. When $M^2 = 1$, the equation is identical to that of a Gaussian laser beam.

Three or more measurements of the spot size at different locations give data points to fit the above equation to find values for w_0 , M^2 , and z_0 . The following method simplifies the real laser equation into a linear equation and uses a least-squares parabola fit.

Using the substitutions,

$$\begin{aligned} x &= z, \\ y(x) &= w^2(z), \\ A &= (M^2)^2 \frac{\lambda^2}{\pi^2 w_0^2}, \\ B &= -2z_0 A, \text{ and} \\ C &= w_0^2 + Az_0^2, \end{aligned}$$

the real laser beam spot size equation can be written as

$$y(x) = Ax^2 + Bx + C. \quad (\text{A-2})$$

Once A , B , and C are found, the beam location, waist, and M^2 are given by,

$$z_0 = -\frac{B}{2A},$$

$$w_o = \sqrt{C - Az_0^2}, \text{ and}$$

$$M^2 = \frac{\pi w_o}{\lambda} \sqrt{A}.$$

To find the coefficients A , B , and C , use the following numerical method as outlined by Matthews and Fink.¹⁴ Given $\{(x_k, y_k)\}_{k=1}^N$ are N points, and abscissas are distinct, the coefficients of the least squares parabola, $y(x) = Ax^2 + Bx + C$, are the solution values of the linear system:

$$\begin{aligned} \left(\sum_{k=1}^N x_k^4\right)A + \left(\sum_{k=1}^N x_k^3\right)B + \left(\sum_{k=1}^N x_k^2\right)C &= \sum_{k=1}^N y_k x_k^2 \\ \left(\sum_{k=1}^N x_k^3\right)A + \left(\sum_{k=1}^N x_k^2\right)B + \left(\sum_{k=1}^N x_k\right)C &= \sum_{k=1}^N y_k x_k \\ \left(\sum_{k=1}^N x_k^2\right)A + \left(\sum_{k=1}^N x_k\right)B + NC &= \sum_{k=1}^N y_k \end{aligned} \quad (\text{A-3})$$

In this application, x is the location of the measurement and y is the spot size of the laser beam at that location. The following Matlab code performs these calculations.

```
function [m2,w0,z0]=Msquared(F,wavelength)
% This function computes the M^2 value of a laser beam according to
% Siegman, SPIE vol 1224, 1990 p. 8
% W^2=W0^2+M2^2*lambda^2/pi^2/W0^2*(Z-Z0^2)^2
% Input-
% F = Nx2 matrix where column 1 are positions(cm) and column 2 are
% corresponding diameters [mm]
% wavelength = wavelength of beam [nm]
% Output-
% m2 = M^2 value of the real laser beam
% w0 = Waist size of the beam [m]
% z0 = Location of Waist [m]
% Assumptions:
% At least 3 data points were taken
```

```

% Abscissas are distinct
% Beam waist lies between two of the data points

mm=1e-3;
cm=1e-2;
nm=1e-9;
lambda=wavelength*nm;

X=F(:,1); % X = Distances from the waist or 'Z'
X=cm.*X;
Y=F(:,2); % Y = Spot size or W
Y=Y/2*mm;
y=Y.^2;

n=length(X);

sumx4=sum(X.^4);
sumx3=sum(X.^3);
sumx2=sum(X.^2);
sumx1=sum(X);

sumy1=sum(y);
sumy1x1=sum(y.*X);
sumy1x2=sum(y.*X.^2);

G=[sumx4 sumx3 sumx2 sumy1x2;sumx3 sumx2 sumx1 sumy1x1;sumx2
sumx1 n sumy1];
H=rref(G);

a=H(1,4);
b=H(2,4);
c=H(3,4);

z0=-b/(2*a);
w0=sqrt(c-a*z0^2);
m2=sqrt(pi^2*w0^2*a/lambda^2);

Z=(X(1,1):.01:X(n,1));
figure (1)
plot(X,Y,'+')
xlabel('Position [meter]')
ylabel('Spot Size [meter]')
title('Spotsize vs Position ')
hold on
plot(Z,sqrt(a.*Z.^2+b.*Z+c))

```

Appendix B: Intensity Stabilization using a GaAs Wafer

This appendix outlines an idea that has the potential to stabilize the intensity of a free-running laser operating in the near IR. As seen in Figure 22, the free running laser pulse has a number of spikes and a width of about 50 μ sec. Since the FND-100 has a negative bias, larger intensity is in the downward direction.

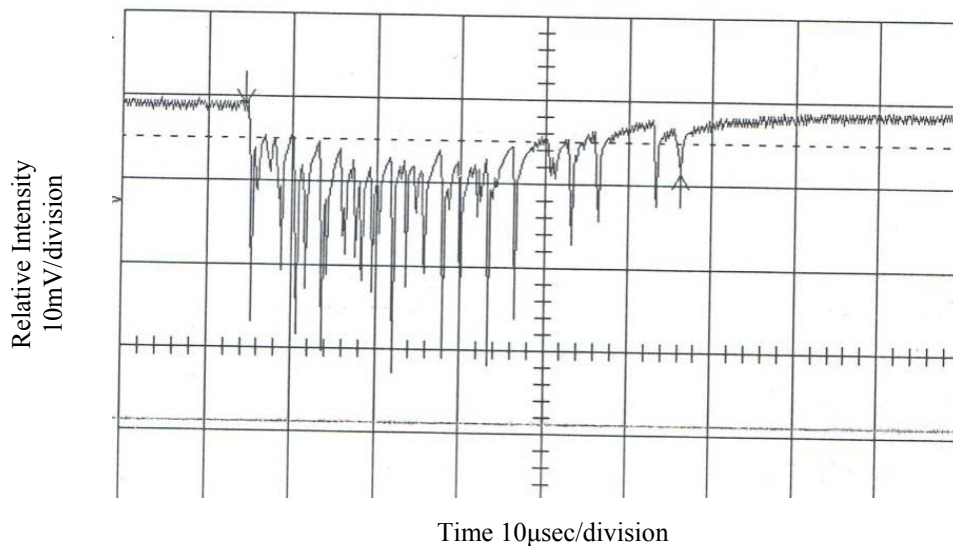


Figure 22. Free running laser pulse comprised of a number of spikes and a width of about 50 μ sec.

It was thought that use a GaAs wafer could reduce the intensity fluctuations associated with the spiking through the nonlinear effect of two-photon absorption. GaAs has a bandgap of 1.42eV. The energy of a photon from the laser operating at 1.06 μ m is about 1.17eV. Since the bandgap of GaAs is higher than the energy of the photon, the GaAs appears transparent under normal conditions. The idea behind two-photon absorption is that two photons may be absorbed together because their combined energy is greater than the bandgap. The probability of two-photon absorption increases as the

intensity of the laser beam increases. Thus, two-photon absorption in GaAs could help reduce the intensity fluctuation of the laser because there would be more absorption in the GaAs wafer at a peak in the pulse, but less absorption at when the intensity is lower.

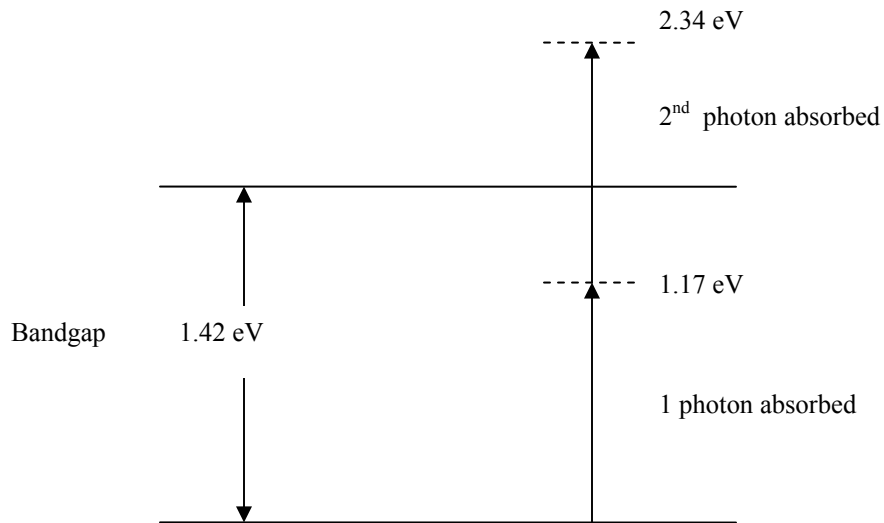


Figure 23. Two-photon absorption in GaAs that has a bandgap of 1.42 eV.

Figure 24, shows the test used to determine if a GaAs wafer would decrease the spikes in intensity of the laser pulse. A 400 μ m thick, undoped GaAs wafer with (100) orientation is set at Brewster's angle. An FND-100 placed before the wafer and a second FND-100 placed after the wafer are read simultaneously on an oscilloscope. After testing with the oscilloscope, the second beam block is removed so that energy measurements can be taken. Energy measurements were taken with the GaAs wafer, and with the GaAs wafer removed.

Since the response from an FND-100 depends on the location, the volts per division for one FND-100 was scaled so that the peaks of the pulses looked nearly equal as viewed on the oscilloscope. The ratio between peak and valley stayed the same according to both detectors. From the response seen on the oscilloscope there was no advantage of using the GaAs wafer.

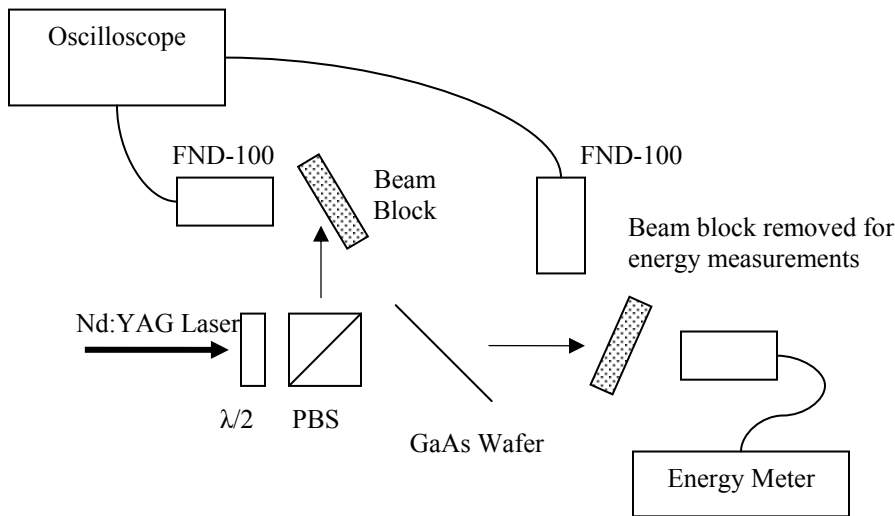


Figure 24. Setup testing the effectiveness of a GaAs wafer to reduce spikes in a free running laser pulse.

A second test took energy measurements with and without the wafer. Twenty single-shot measurements of energy were taken. With the wafer, energy measurements ranged from 344 – 368 μJ , a range of 24 μJ , an average of 355.6 μJ , and a standard deviation of 6.7 μJ . The GaAs was removed and the intensity of the laser reduced so that the energy response would be in the same range. With the GaAs removed, energy measurements

ranged from 338 – 349 μJ , a range of 11 μJ , an average of 342 μJ , and a standard deviation of 3.8 μJ .

The results of these two tests did not give sufficient evidence that two-photon absorption in the GaAs wafer played a role in reducing the spiking in the free-running laser pulse. Therefore, the wafer was not used in the Raman fiber laser experiments.

References

- ¹ D. L. Lamberson, "Keynote Address To Fifteenth Annual Solid State and Diode Laser Technology Review," *SSDLTR 2002 Technical Digest*, PLEN 1, 2002.
- ² T. H. Russell, S. M. Willis, M. B. Crookston, and W. B. Roh, "Stimulated Raman Scattering in Multi-Mode Fibers and its Application to Beam Cleanup and Combining," *JNOPM*, vol. 11, no. 3, pp. 303-316, 2002.
- ³ P. L. Baldeck, F. Raccach, and R. R. Alfano, "Observation of self-focusing in optical fibers with picosecond pulses," *Opt. Lett.*, vol. 12, no. 8, pp. 588-589, 1987.
- ⁴ A. B. Grudinin, E. M. Dianov, D. V. Korbkin, A. M. Prokhorov, and D. V. Khaidarov, "Nonlinear mode coupling in multimode optical fibers; excitation of femtosecond-range stimulated-Raman-scattering solitons," *JETP Letters*, vol. 47, pp. 356-359, 1988.
- ⁵ K. S. Chiang, "Stimulated Raman scattering in a multimode optical fiber: evolution of modes in Stokes waves," *Opt. Lett.*, vol. 17, pp. 352-354, 1992.
- ⁶ B. C. Rodgers, T. H. Russell, and W. B. Roh, "Laser beam combining and cleanup by stimulated Brillouin scattering in a multimode optical fiber," *Opt. Lett.*, vol. 24, pp. 1124-1126, 1999.
- ⁷ T. H. Russell and W. B. Roh, "Threshold of second-order stimulated Brillouin scattering in optical fiber", *J. Opt. Soc. Am. B*, vol. 19, no. 10, pp. 2341-5, Oct. 2002.
- ⁸ G. P. Agrawal, *Nonlinear Fiber Optics*, 3 ed. San Diego: Academic Press, Inc., 2001.
- ⁹ R. H. Stolen, E. P. Ippen, and A. R. Tynes, "Raman Oscillation in Glass Optical Waveguide", *Appl. Phys. Lett.*, vol. 20, 1972.
- ¹⁰ B. Holtkamp and D. Kuizenga, "High-power Raman fiber lasers test components", *Laser Focus World*, pp. 95-99, June 2001.
- ¹¹ G.P. Agrawal, *Applications of Nonlinear Fiber Optics*, San Diego: Academic Press, Inc., 2001.
- ¹² A. E. Siegman, "New developments in laser resonators," in *Optical Resonators, Proc. SPIE*, vol. 1224, pp. 2-14, 1990.

- ¹³ *BeamView Analyzer Analog 2.2 Digital 3.0 User's Guide*, Coherent Auburn Division, Auburn, CA, 2001.
- ¹⁴ J. H. Matthews and K. D. Fink, *Numerical Methods Using MATLAB*, 3 ed. Upper Saddle River, NJ: Prentice Hall, 1999.

Vita

Lieutenant Matthew B. Crookston graduated from Rangely High School in Rangely, Colorado. He attended Brigham Young University in Provo, Utah for a year before serving a two-year mission for the Church of Jesus Christ of Latter-day Saints in South Carolina. Returning to Brigham Young University to complete his undergraduate studies in physics, he also joined the AFROTC Detachment 855. In the spring of 2001 he graduated from Brigham Young University, married his college sweetheart, and earned his Commission into the United States Air Force.

In August of 2001, Lieutenant Crookston's first assignment was to the Graduate School of Engineering and Management, Air Force Institute of Technology to pursue a Masters degree in Applied Physics. Upon graduation, his follow on assignment is to the Air Force Research Labs at Hanscom AFB, Massachusetts.

REPORT DOCUMENTATION PAGE				Form Approved OMB No. 074-0188	
<p>The public reporting burden for this collection of information is estimated to average 1 hour per response, including the time for reviewing instructions, searching existing data sources, gathering and maintaining the data needed, and completing and reviewing the collection of information. Send comments regarding this burden estimate or any other aspect of the collection of information, including suggestions for reducing this burden to Department of Defense, Washington Headquarters Services, Directorate for Information Operations and Reports (0704-0188), 1215 Jefferson Davis Highway, Suite 1204, Arlington, VA 22202-4302. Respondents should be aware that notwithstanding any other provision of law, no person shall be subject to a penalty for failing to comply with a collection of information if it does not display a currently valid OMB control number.</p> <p>PLEASE DO NOT RETURN YOUR FORM TO THE ABOVE ADDRESS.</p>					
1. REPORT DATE (DD-MM-YYYY) 10-03-2003		2. REPORT TYPE Master's Thesis		3. DATES COVERED (From – To) Jun 2002 – Mar 2003	
4. TITLE AND SUBTITLE SINGLE-MODE RAMAN FIBER LASER IN A MULTIMODE FIBER				5a. CONTRACT NUMBER	
				5b. GRANT NUMBER	
				5c. PROGRAM ELEMENT NUMBER	
6. AUTHOR(S) Crookston, Matthew B., 2 nd Lieutenant, USAF				5d. PROJECT NUMBER 02-265	
				5e. TASK NUMBER	
				5f. WORK UNIT NUMBER	
7. PERFORMING ORGANIZATION NAMES(S) AND ADDRESS(S) Air Force Institute of Technology Graduate School of Engineering and Management (AFIT/EN), Building 640 2950 Hobson Way Wright Patterson AFB OH 45433-7765				8. PERFORMING ORGANIZATION REPORT NUMBER AFIT/GAP/ENP/03-03	
9. SPONSORING/MONITORING AGENCY NAME(S) AND ADDRESS(ES) Air Force Office of Scientific Research (AFOSR/NE) Attn: Dr. Howard Schlossberg 801 N. Randolph Street Arlington VA 22203-7549 telephone: (703) 696-7549 e-mail: howard.schlossberg@afosr.af.mil				10. SPONSOR/MONITOR'S ACRONYM(S)	
				11. SPONSOR/MONITOR'S REPORT NUMBER(S)	
12. DISTRIBUTION/AVAILABILITY STATEMENT APPROVED FOR PUBLIC RELEASE; DISTRIBUTION UNLIMITED.					
13. SUPPLEMENTARY NOTES					
14. ABSTRACT The feasibility of a transverse single-mode Raman fiber laser using a multimode fiber has been investigated. The Raman fiber laser operates in low-order transverse modes despite the fact the fiber supports multimode beam propagation. The performance characteristics of the Raman fiber laser are compared with those of the single-pass SRS beam.					
15. SUBJECT TERMS Stimulated Raman Scattering, Raman Laser, Optical Fiber, Beam Cleanup, Multimode Fiber					
16. SECURITY CLASSIFICATION OF:			17. LIMITATION OF ABSTRACT	18. NUMBER OF PAGES	19a. NAME OF RESPONSIBLE PERSON
a. REPORT	b. ABSTRACT	c. THIS PAGE			Dr. Won B. Roh (AFIT/ENP)
U	U	U	UU	53	19b. TELEPHONE NUMBER (Include area code) (937) 255-6565, ext 4509; e-mail: Won.Roh@afit.edu